Cerebral Cortex Advance Access published November 10, 2004

Focal Decline of Cortical Thickness in Alzheimer's Disease Identified by Computational Neuroanatomy

Jason P. Lerch[1], Jens C. Pruessner[1,2], Alex Zijdenbos[1], Harald Hampel[2], Stefan J. Teipel[2] and Alan C. Evans[1]

[1]McConnell Brain Imaging Centre, Montreal Neurological Institute, McGill University, Montreal, Quebec, Canada, and [2]Alzheimer Memorial Center, Dementia Research Section and Memory Clinic, Department of Psychiatry, Ludwig-Maximilian University, Munich, Germany

Alzheimer's disease (AD) is characterized by a heterogeneous distribution of pathological changes throughout the brain. Magnetic resonance imaging can be used to investigate the regional distribution of cortical atrophy in AD *in vivo*. One marker for the disease-specific atrophy is the thickness of the cortical mantle across the brain, obtained with automated 3-D image processing. Here, we present data from 36 subjects (17 controls and, 19 patients diagnosed as probable AD) investigated for cortical thickness across the entire brain. We show significant cortical thickness decline in AD in temporal, orbitofrontal and parietal regions, with the most pronounced changes occurring in the allocortical region of the medial temporal lobes, outlining the parahippocampal gyrus, and representing a loss of >1.25 millimeters of cortical thickness. Moreover, focal cortical areas decline with progression of the disease as measured by time from baseline scan as well as the Mini-Mental State Exam. The results demonstrate the ability of this method to detect changes in cortical thickness in AD, across the entire brain, without need of prior anatomical definitions. The regional distribution of changes reported here is consistent with independent findings on the distribution of neuropathological alterations in AD. Using cortical thickness, moreover, we provide a direct quantitative index of atrophy in the disease.

Keywords: Alzheimer's disease, automated 3-D image analysis, cortical thickness, MRI, neuroinformatics, neuropathology

Introduction

Alzheimer's disease is characterized by the formation of neurofibrillary plaques and tangles, and neuronal loss across the central nervous system (Small *et al.*, 2002). The histopathological changes show a characteristic sequence, with the entorhinal cortex and the hippocampus being among the first affected regions of the brain, followed by selected regions of the neocortex (Braak and Braak, 1991, 1996; Juottonen *et al.*, 1998). Cognitive decline correlates with cortical atrophy (Mungas *et al.*, 2002), which can be investigated with magnetic resonance imaging (MRI) *in vivo*.

MRI provides insight into the temporal sequence of AD-related regional atrophy, using region specific as well as global search algorithms. Within region specific protocols, recent effort has focused on using MRI to detect early morphological changes in AD pathology; attention has specifically focused on developing precise segmentation protocols for the early affected temporal lobe structures such as the entorhinal cortex (EC) or the hippocampus (HC) (Van Hoesen, 1995; de Leon *et al.*, 1997; Mori *et al.*, 1997; Krasuski *et al.*, 1998; De Toledo-Morrell *et al.*, 2000).

In comparison, whole brain imaging analysis allows detection of changes throughout the entire cerebrum. So far, the methodology of whole brain analysis approaches has been restricted to voxel-based morphometry (VBM) (Ashburner and Friston, 2000), implemented volumetrically (Baron *et al.*, 2001) across the cortex (Thompson, 1989; Thompson *et al.*, 2001), or as deformation analysis in longitudinal datasets (Good *et al.*, 2002). In VBM, the concepts of gray matter density and gray matter concentration are central for the interpretation of the results; however, voxel density at any one point for any one subject is, unlike cortical thickness, meaningless.

Using specific algorithms to analyze cortical thickness across the entire cortex is a complementary method to the established research paradigms, offering a direct quantitative index of cortical atrophy that can be applied to single subjects and to group analysis. Cortical atrophy is reflected in a loss of gray matter which will result in a reduction of cortical thickness. Measuring cortical thickness across the entire cerebrum establishes a marker for the AD-related cortical atrophy.

Materials and Methods

Thirty-six subjects were investigated. MRI scans were acquired from, 19 patients with a combined 31 acquisitions (up to three scans per subject). The patients had the clinical diagnosis of probable AD according to the NINCDS-ADRDA (McKhann *et al.*, 1984). For comparison of baseline MRI measures, 17 healthy volunteers with one acquisition each were recruited and subsequently scanned using identical acquisition parameters. Patients were recruited from the Department of Psychiatry, Alzheimer Memorial Center, Dementia and Imaging Research Group, University of Munich, Germany. Further sociodemographic information of the subjects is shown in Table 1. Cognitive impairment in the AD patients was assessed using the Mini Mental State Examination (MMSE) (Folstein *et al.*, 1975). The average MMSE score in the Alzheimer group was 21.2 (10–29). In the control group, the MMSE average score was 29.3 (range 28–30).

Significant medical co-morbidity in the AD patients and controls was excluded by interviews on medical history, physical and neurological examination, psychiatric evaluation, chest X-ray, ECG, EEG, brain MRI and laboratory tests (complete blood count, sedimentation rate, electrolytes, glucose, blood urea nitrogen, creatinine, liver-associated enzymes, cholesterol, HDL, triglycerides, antinuclear antibodies, rheumatoid factor, VDRL, HIV, serum B12, folate, thyroid function tests and urine analysis). None of the AD patients had hypertension or diabetes. All subjects or the holders of their Durable Power of Attorney provided written informed consent for the study. The protocol was approved by the Ethical Review Board of the Faculty of Medicine, Ludwig Maximilian University, Munich, Germany.

MRI examinations were performed on a 1.5 T Siemens Magnetom Vision MRI scanner (Siemens, Erlangen, Germany). All subjects were investigated with a volumetric T1-weighted sagittal oriented MRI sequence (T_R = 11.6 ms, T_E = 4.9 ms, resolution = 0.94 × 0.94 × 1.2 mm). The rectangular field of view (FOV) for the sagittal images was 256 mm (SI) × 204 mm (AP). Additionally, an axial-oriented fast FLAIR sequence (T_R = 9000 ms, T_E = 110 ms, resolution = 0.94 × 0.94 × 6 mm) was obtained. For the purpose of this study, only the T1-weighted images entered further processing. The native MRI were registered into standardized stereotaxic space using a linear transformation (Collins

Table 1
Demographics of the study population

	No. of subjects	No. of scans	Age	MMSE
Controls	17	17	61.0 ± 9.1	29.3 ± 0.6
Patients	19	31	68.8 ± 6.9	21.2 ± 4.6

Table 2
Results sorted by *t*-statistics

Location	Talairach coordinates			*t*-statistics	Difference (mm)	% atrophy
	x	*y*	*z*			
PHG	27	2	−39	−6.7	−1.25 ± 0.22	22 ± 3.8
ITG	−47	−55	−16	−5.3	−1.00 ± 0.18	22 ± 4.0
MOG	−13	31	−21	−4.5	−0.86 ± 0.23	18 ± 4.9
STG	59	−42	14	−4.4	−0.65 ± 0.14	17 ± 2.7
Post. Cing.	4	−30	37	−4.3	−0.86 ± 0.19	22 ± 5.0
LOG	−20	−99	0	−4.1	−1.03 ± 0.25	24 ± 5.8
MTG	63	−39	−14	−3.8	−0.85 ± 0.22	20 ± 5.2
Lt. IFG	−46	36	11	−3.7	−0.76 ± 0.22	22 ± 5.6
Ant. cing.	−11	50	5	−3.4	−0.95 ± 0.28	19 ± 5.8

Ant. cing., anterior cingulated; ITG, inferior tempral gyrus; LOG, lateral occipital gyrus; Lt IFG, left inferior frontal gyrus; MFG, middle frontal gyrus; MOG, medial orbital gyrus; MTG, middle temporal gyrus; PHG, parahippocampal gyrus; Post. cing., posterior cingulated; STG, superior temporal gyrus.

et al., 1994). Simultaneously, the images were corrected for non-uniformity artifacts (Sled *et al.*, 1998). The registered and corrected volumes were segmented into white matter, gray matter, cerebrospinal fluid and background using an advanced neural net classifier (Zijdenbos *et al.*, 2002). The white and gray matter surface were then fitted using deformable models (MacDonald *et al.*, 2000), resulting in two surfaces with 81 920 polygons each. The surface deformation algorithm works by first fitting the white matter surface, then expanding outward to find the gray matter CSF intersection. One characteristic of this procedure is that each vertex of the white matter surface is closely related to its gray matter surface counterpart; cortical thickness can thus be defined as the distance between these linked vertices. The relevant parts of the processing pipeline are shown schematically in Figure 1.

In order to improve the ability to detect population changes, each subject's cortical thickness map was blurred using a 20 mm surface based blurring kernel (Chung *et al.*, 2002). Diffusion smoothing, unlike the volumetric blurring used in VBM, follows the curvature of the surface and thus respects anatomical boundaries. Twenty millimeters was chosen as the kernel size in order to maximize statistical power while still minimizing false positives.

Statistical analysis was performed at every vertex, regressing cortical thickness against clinical state, MMSE scores, or time from baseline. Multiple time-points were used where available in order to provide greater stability in the estimation of the fixed effects than a purely cross-sectional model would have allowed. Linear mixed models using the restricted maximum likelihood (REML) estimation method were employed to account for the within subject correlations present due to the repeated acquisitions in the AD cohort (Pinheiro and Bates, 2000). Mixed models extend linear models by incorporating random effects, which can best be regarded as an additional error term. The model used is the following:

$$Y_i = X_i\beta + Z_i b_i + \varepsilon_i,\ i = 1,\ldots,M$$

where β is the vector of fixed effects, b_i, $i = 1,\ldots,M$ is the vector of random effects describing a shift in the intercept for each subject (M taking the value of either 19 or 36, depending on whether only the patients or all subjects were used), X_i (of size $n_i \times p$) and Z (of size $n_i \times q$) are known fixed-effects and random-effects regressor matrices and ε_i is the n_i dimensional within group error vector, where n_i takes on values between 1 and 3, describing the number of acquisitions per subject. y_i is the estimated cortical thickness vector for subject i. Each of the

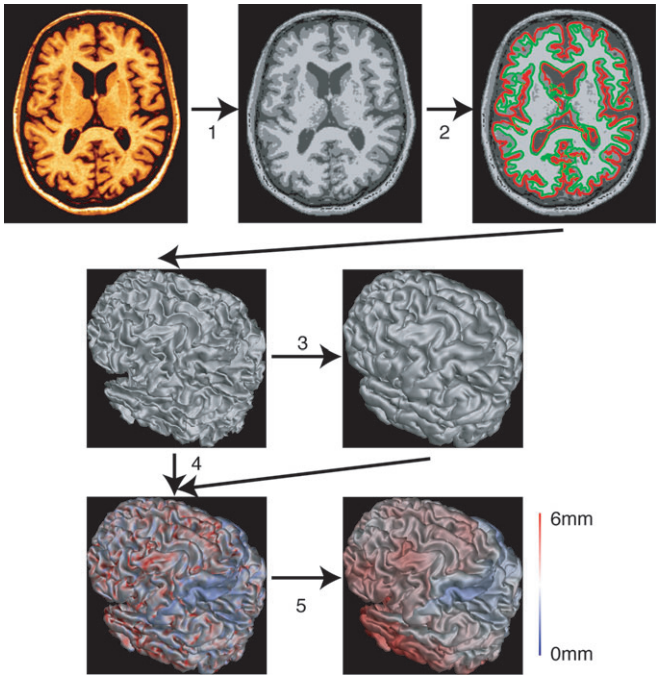

Figure 1. An overview of the steps involved in cortical thickness analysis. First, the images are non-uniformity corrected and registered into stereotaxic space. They are then classified (1) and fit with a white matter surface (2). The gray surface is found by expanding out from the white (3). Cortical thickness is measured at every vertex (4), and blurred using a 20 mm surface-based kernel (5).

statistical models used age as a covariate, thereby controlling for the main effects of age on the dependent variables; the value of p is therefore 3. The random-effects matrices (Z) included the intercept term; the value of q is therefore 1. For the regression with the MMSE scores, only the AD subjects were selected in order to avoid confounding of the clinical state with the MMSE analysis.

To illustrate with an example, the matrices for the MMSE analysis would be:

$$X_1 = \cdots = X_{19} = \begin{bmatrix} 1 & 66.9 & 24 \\ 1 & 67.8 & 20 \\ 1 & 69.5 & 20 \end{bmatrix}, \quad Z_1 = \cdots = Z_{19} = \begin{bmatrix} 1 \\ 1 \\ 1 \end{bmatrix}$$

with the example subject 19 being one subject with three acquisitions taken at age 66.9, 67.8 and 69.5, and having MMSE scores of 24, 20 and 20 at each respective acquisition. The one-dimensional random effects matrix Z is the intercept for each subject — i.e. a common slope across subjects was assumed, with only the intercepts allowed to vary. For the other analyses (clinical state and time from baseline) the third column of the matrix would change to be a 0 or 1 for control or patient in the clinical state analysis (i.e. 'treatment' contrasts were used) or the time, measured in years, of the follow up scan minus the baseline scan (i.e. for subject 19, these would be 0, 0.9 and 2.6). The terms of β would thus be: β_1, the mean intercept; β_2, for the common effect of age; and β_3, the common effect of MMSE/group/time from baseline. The one-dimensional vector b_i, $i = 1,\ldots,19$ (in the case of the MMSE or time since baseline analysis, since only the 19 patients are considered) or b_i, $i = 1,\ldots,36$ (in the case of the clinical state analysis, since all 36 subjects are considered) describes a shift in the intercept for each subject. In the parlance of the computational system used to solve these equations (Pinheiro and Bates, 2000), the function call is *lme*(*y* ~ *1* + *age* + *MMSE*, *random* = ~*1*|*ID*), where y is the cortical thickness at the vertex in question, *age* is the age at the time of each acquisition, *MMSE* is the MMSE score at the time of each acquisition, the random effect is the intercept and all subjects are grouped by the subject ID.

The resulting statistical maps were thresholded using the false discovery rate (FDR) theory (Genovese *et al.*, 2002) at a q value of 0.05 after pooling the P-values from all regressions run in this analysis.

The interpretation of the maps is therefore that, on average, 5% of the results shown across all regressions are false positives. The figures also show the regression slope, which is the change in millimeters with each unit of measurement (group difference, point of MMSE, or in years).

Cortical thickness methods applied to human magnetic resonance images can be divided into three broad categories. The first measures thickness on a voxel by voxel level, and is illustrated by two papers solving a partial differential equation across the cortex (Jones *et al.*, 2000; Yezzi and Prince, 2003). The second set of methods use advanced versions of the *marching cubes* algorithm, creating two cortical surfaces with variable tesselation (cf. Zeng *et al.*, 1999; Miller *et al.*, 2000). The last group uses deformable models to create white and grey matter cortices, and includes our work outlined above and that of Fischl and colleagues (Fischl and Dale, 2000; Rosas *et al.*, 2002). One characteristic of using deformable models is that the number of polygons will always be identical across subjects, allowing for the easy creation of a surface coordinate system that can be used to run statistical analyses of cortical thickness at every vertex of the surface.

Our cortical thickness algorithm has been validated by comparison to manual measurements (Kabani *et al.*, 2001). Furthermore, extensive analysis of the precision of our cortical thickness analysis framework was recently preformed (Lerch and Evans, 2004). Two tests were run: a study of reliability, where 19 scans of the same subject were processed separately to assess for methodological variability, and a population simulation. In the latter, 50 normal scans were processed. Twenty-five of them had the right superior temporal gyrus (rSTG) artificially thinned by one six-neighbor dilation of the white matter in that region, and that change recovered statistically. In the 19 repeat scans the mean standard deviation across all vertices was 0.27 mm. The population simulation resulted in 93% sensitivity in areas of perfect overlap of the rSTG along with 100% specificity (no single vertex outside of the rSTG was found to be significant between the two groups). This simulation study provides confidence that results shown using the AD data described in this paper are valid.

Results

Group Differences (Normals versus AD)

The results from the analysis clearly show significant differences in cortical thickness between the two groups. The average thickness across the entire cortex was significantly thinner in AD patients (3.1 ± 0.28 mm) compared with controls (3.74 ± 0.32 mm; $t = -3.8$, $P < 0.0007$), resulting in an average difference of 0.47 mm after removal of age effect by regression. Furthermore, the resulting maps of atrophy clearly show region specificity of thickness decline in AD. The most significant changes were found in the medial temporal lobes, the anterior and posterior cingulate region, the frontal lobes, the inferior parietal lobes, the orbitofrontal cortex, and the visual association cortex (Figs 2–4, Table 2). Most of these effects were found bilaterally except for the insula region, where only the left hemisphere appeared significant.

In the frontal lobes, the effects were most pronounced in the left anterior cingulate region (0.95 ± 0.28 mm loss in AD), the dorsolateral prefrontal cortex (0.76 ± 0.22 mm loss), and the orbitofrontal cortex (0.86 ± 0.23 mm). The effects in the dorsolateral prefrontal cortex appeared in the vicinity of Brodmann's area (BA) 45. The effects were stronger in the left than in the right hemisphere. In the parietal lobe, the effects were most pronounced in the posterior cingulate region (0.86 ± 0.19 mm loss in cortical thickness in AD), and the visual association areas (1.0 ± 0.25 mm loss).

The entire medial temporal lobe appeared to be severely affected. The average difference between cortical thickness in AD and in the control group ranged from 0.5 to 1.3 mm, with the strongest differences emerging in the area of the parahippocampal gyrus (PHG). This finding is consistent with the results from recent studies suggesting that the PHG, especially the entorhinal cortex (EC), is affected early in the course of AD (Krasuski *et al.*, 1998; Van Hoesen *et al.*, 2000; Callen *et al.*, 2001). To investigate cortical thickness decline in this area in our subjects more closely, manual segmentation of the structures of the PHG was used to trace the EC in the MRI of all subjects using a recently developed protocol (Pruessner *et al.*, 2002). The labels of the EC from all subjects were then used to create a customized probabilistic map of the EC for the subjects in this study, which was overlaid onto the *t*-statistics map from the thickness analysis. This allowed an accurate evaluation of the decline in cortical thickness within the EC in our study sample. The result of this procedure is shown in Figure 5, indicating that the most striking difference between the two groups occurred in the anterior portion of the EC in the left hemisphere, with a difference of 1.25 ± 0.22 mm in cortical

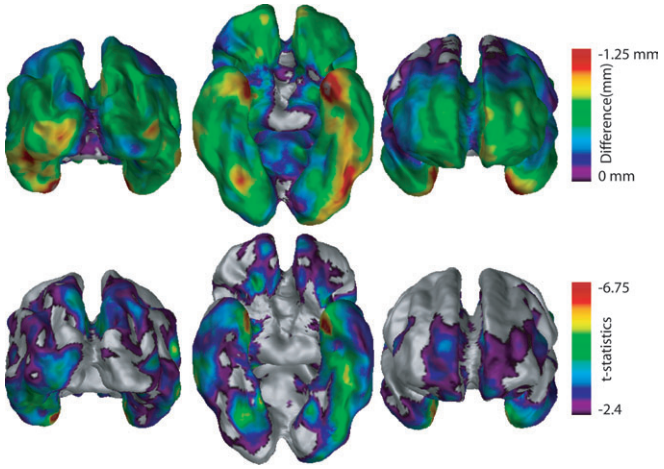

Figure 2. *t*-statistical (lower panel) and cortical thickness (upper panel) difference maps in 19 AD subjects versus 17 controls (age effect removed by regression). Results from the statistical analysis are displayed at each vertex of the surface of a standardized brain in terms of *t*-statistical color maps as well as color maps displaying the estimated cortical thickness difference in millimeters (the regression slope) between the two groups. Significant differences can be seen in the temporal lobes, especially the entorhinal and perirhinal cortices, as well as medial frontal and parietal lobes and left associative visual areas.

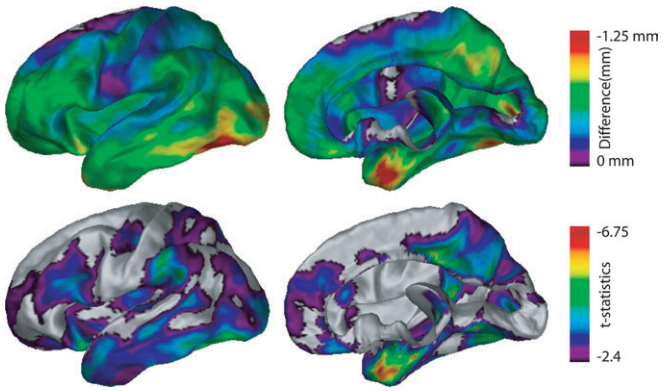

Figure 3. *t*-statistical (lower panel) and cortical thickness (upper panel) difference maps in 19 AD subjects versus 17 controls (age effect removed by regression). The display emphasizes the differences in the left lateral and right medial views. Significant differences can be seen in the posterior and anterior cingulate, the left dorsolateral prefrontal cortex, most of the temporal lobes, and the left supramarginal gyrus.

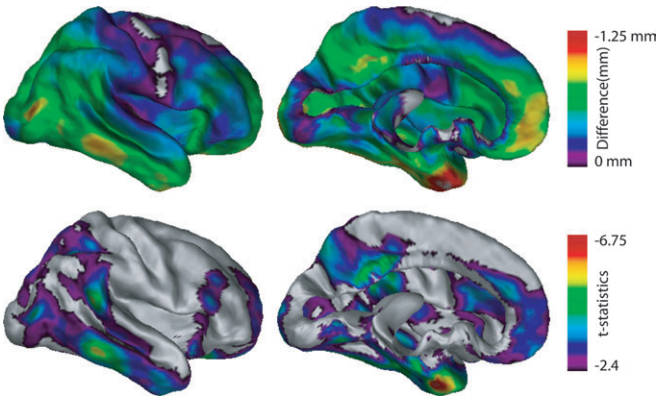

Figure 4. *t*-statistical (lower panel) and cortical thickness (upper panel) difference maps in 19 AD subjects versus 17 controls (age effect removed by regression). The display emphasizes the differences right lateral and left medial views. Significant differences can be found throughout the temporal lobes, the posterior and anterior cingulate. Compared with the left hemisphere, the difference in the supramarginal gyrus and the dorsolateral prefrontal cortex is reduced.

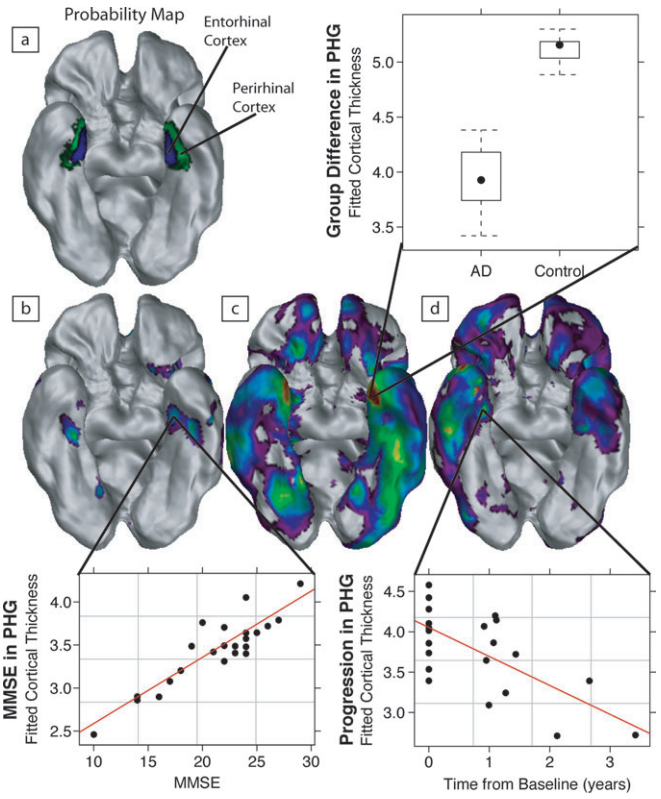

Figure 5. Regional analysis using the cortical thickness methodology in AD versus normal controls displaying differences in the entorhinal cortex. The four cortical views show: (*a*) the probability maps of the entorhinal and perirhinal cortices in this population; (*b*) the *t*-statistics of the MMSE regression; (*c*) the group analysis; and (*d*) the time difference from baseline. The color scales are the same as in Figures 2–4, 6 and 7 respectively. The graphs illustrate the effects at the vertex indicated by the black lines. Atrophy of the PHG is clearly implicated in each of the three analyses shown.

thickness between the two groups. The lateral temporal lobes also showed significant interaction with clinical state, with a peak of 0.8 ± 0.22 mm in the left medial temporal gyrus (BA 21).

In the parietal and occipital lobes, significant differences further appeared in the transition area between parietal and occipital lobes in the area of the visual association cortex (BA 18–19; between 0.4 – 1.0 mm loss of cortical thickness in the AD group). Interestingly, the primary visual cortex (BA 17) appeared to be spared, showing no interaction with group (t = –1.6).

Regression of Cortical Thickness versus MMSE

In order to investigate whether cortical thickness measures vary with disease progression in the AD patients, a regression of cortical thickness against the MMSE score was performed in the AD patients at every vertex of the surface model. Mean cortical thickness was marginally associated with MMSE scores (t = 2.24, P = 0.06). Regionally, however, it was found that lower MMSE scores were associated with significantly thinner cortical thickness in the bilateral PHG, the left superior temporal gyrus, left insula, and left anterior cingulate gyrus (Fig. 6).

Regression of Cortical Thickness versus Progression

Further analysis of the effect of disease progression was performed by regressing cortical thickness against the time difference from baseline in the follow-up scans within the AD cohort. There was a significant correlation between time from baseline and thickness (t = –3.47, P = 0.006) featuring a decline of 0.18 mm per year. Significant regional correlations were found in the anterior temporal lobes including the parahippocampal gyrus, the anterior frontal lobes, and the anterior cingulate (Fig. 7). A post-hoc test was also conducted to ascertain the rate of thinning in cortical areas that featured an initial group difference versus those where the Alzheimer's patients did not have significantly thinner cortex than the normal controls. Both these areas declined significantly with time from baseline; the rate was faster in cortical regions which were also significantly thinner in the patients (0.21mm per year, t = –4, P = 0.004) than the rest of the cortex (0.16mm per year, t = –3.4, P = 0.009).

Discussion

We used a fully automated method to measure cortical thickness across the entire brain to investigate differences in a group of AD patients versus age-matched controls. We further investigated the correlation between cortical thickness and MMSE scores as well as time since baseline in the patient population.

Our results clearly show AD related decline in cortical thickness in multiple areas of the brain, many of which have been reported in previous MR studies. Cortical thickness of the medial temporal lobes was most severely reduced in AD patients, and, within the medial temporal lobes, the parahippocampal gyrus was most affected. This is consistent with previous MR and histopathological studies showing that this region of the brain is affected early and profoundly in the course of the disease (Juottonen *et al.*, 1999; Xu *et al.*, 2000). The results from this study extend previous findings by showing that in the left hemisphere, the posterior portions of the PHG also seem to be strongly affected in AD. For the anterior portion of the PHG, in the area of the entorhinal cortex, the most significant differences occurred in the left hemisphere, though the effects were largely bilateral.

Cortical atrophy in AD is not limited to the medial temporal lobe; the remaining limbic system, the lateral temporal lobes, and certain associative visual areas correlate significantly with

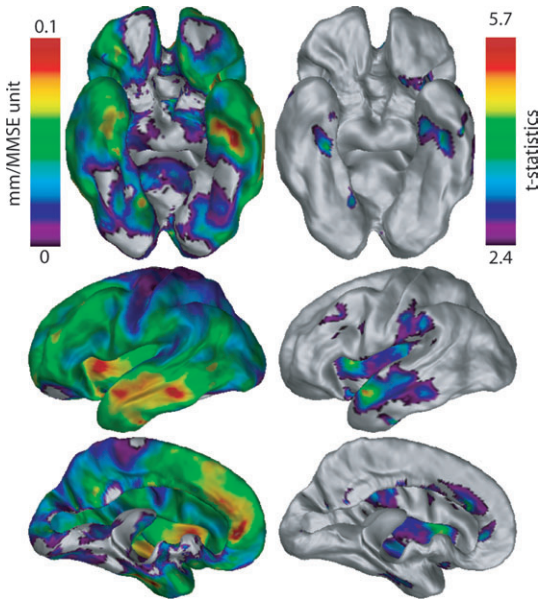

Figure 6. *t*-statistical (right column) and cortical thickness (left column) maps of the MMSE regression against cortical thickness in 19 AD subjects. Significant correlations can be seen in the lateral temporal lobes, the left insula, left anterior cingulate and bilateral para-hippocampal gyri.

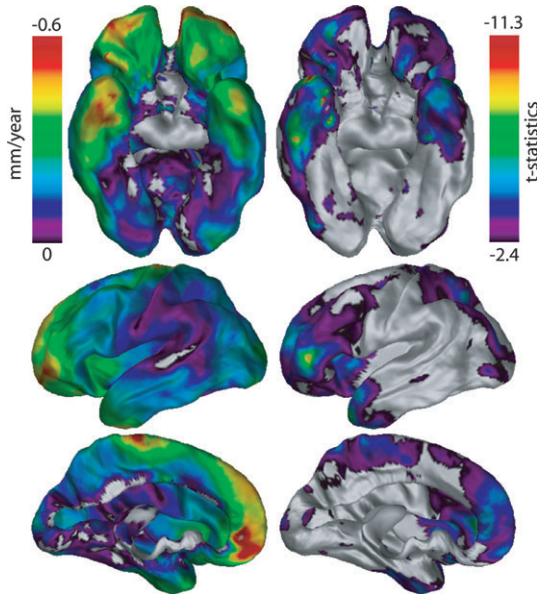

Figure 7. *t*-statistical (right column) and cortical thickness (left column) maps of the regression against time from baseline. Significant correlations can be seen in the anterior temporal lobes, anterior frontal lobes, and lateral posterior cortex.

the disease as well. The finding of significant cortical thickness decline in the area of the visual association cortex is consistent with other studies showing this region to be strongly affected by AD (Cronin-Golomb *et al.*, 1991; Thulborn *et al.*, 2000), as are the results in the lateral temporal lobes (Busatto *et al.*, 2003). Within the limbic system the orbito-frontal cortex (Van Hoesen *et al.*, 2000) and the anterior and posterior cingulate cortices (Valla *et al.*, 2001; Matsuda *et al.*, 2002) have also been shown to correlate with the disease in ways that support the results of this study. Combined with spared areas of the cortex, such as the motor, sensory and primary visual cortices (BA17) (Buckner *et al.*, 2000; Rizzo *et al.*, 2000; Prvulovic *et al.*, 2002), a pattern of atrophy in AD emerges that is focal to multiple cortical areas while centered on the medial temporal lobes.

The results from the MMSE regression within the AD group indicate that the decline in the PHG is correlated with the MMSE score (Fields *et al.*, 1992). Significant associations between MMSE scores and cortical thickness were found in bilateral medial temporal areas as well as temporal, anterior cingulate, and insular regions of the left hemisphere. The results demonstrate that cortical thickness analysis can be used to link clinical information with decline in particular cortical areas when available. In the case of MMSE scores, the significant findings with cortical atrophy were left hemisphere dominant. Progression as measured by time from baseline in repeated scans showed a more significant effect than the MMSE analysis, indicating continuing atrophy that is not entirely captured by changes in cognitive state as captured by the MMSE. Progressive atrophy was particularly strong in the anterior frontal and temporal lobes as well as the posterior cingulate. Cortical areas which were significantly thinner in the patients thinned at a faster rate than those that were not, though this difference was small and would therefore suggest that the entire cortex is declining with disease progression. The longitudinal aspect of our analysis should be explored in greater detail and compared to non-linear registration methods that have recently been used in the analysis of AD populations and normal aging (Fox *et al.*, 2000; Scahill *et al.*, 2002, 2003).

AD is commonly subdivided into six stages representing advancing pathology as defined by the progression of neurofibrillary tangles (NFTs) and senile placques (Braak and Braak, 1991, 1996). The patients used in this study were diagnosed with probable AD according to NINCDS-ARDRA criteria and thus believed to be in stage V or VI (Nagy *et al.*, 1999). These two end stages, known as the neocortical stages, feature plaque and NFT involvement in virtually all subdivisions of the cerebral cortex with a particular emphasis on association areas and the medial temporal lobes. NFT presence is strongly correlated with neuronal loss and cortical atrophy (Gomez-Isla *et al.*, 1997; Grignon *et al.*, 1998). Moreover, increased duration of NFT presence is associated with increased atrophy (Grignon *et al.*, 1998). This leads to the hypothesis that, in patients diagnosed with probable AD, cortical areas involved earlier in the disease progression will show greater atrophy than areas involved later (Gomez-Isla *et al.*, 1997). Our results, which reveal greatest MRI detectable atrophy in areas implicated earlier (such as the entorhinal cortex), largely support this hypothesis. The ability to stage AD based on in-vivo imaging should be investigated further. Moreover, some of the findings in this study may be due to the small sample size, since occasional atypical representation of AD (such as the visuo-spatial variant; cf. Cronin-Golomb *et al.*, 1991) may have an undue influence on our results. This analysis should therefore be replicated in a larger sample.

The major difference between previous findings and the results obtained in this study lies in the use of the cortical thickness analysis technique. This strategy has a number of advantages when compared with other MR methods used to investigate AD with MRI. Cortical thickness analysis allows searching for associations between the depth of the cortex and sociodemographic, clinical or psychological variables across the entire surface of the brain. It shares this advantage with other global search algorithms like VBM and deformation field

analysis. Unlike VBM, however, it is based on the description of the actual thickness of the cortex in millimeters and thus allows meaningful quantitative description of the results (difference in cortical thickness in millimeters). The major disadvantage is that the focus is entirely on the cortex; changes in subcortical structures, white matter or cerebro-spinal fluid will not be picked up.

Finally, cortical thickness analysis is fully automated and thus reaches 100% operator independence. The results are operator-independent and do not rely on the correct interpretation of regional anatomical variations, in contrast to manual segmentation protocols.

Cortical thickness analysis may serve as a surrogate marker for the neuronal loss that accompanies the histopathological changes in the cortex which occur in AD and their temporal ordering. For example, the highly significant findings in the PHG, in the area of the EC, support the view (Juottonen *et al.*, 1999; Xu *et al.*, 2000) about the importance of medial temporal lobe morphometry in the diagnosis of AD. Future studies can compare the relative efficacy of cortical thickness measures with volumetric analyses of the hippocampus (Pruessner *et al.*, 2001).

Continuing work will investigate associations between cortical thickness and other sociodemographic or clinical variables. Owing to its fully automatic implementation, the method can be used to characterize the healthy and pathological ranges of cortical thickness in specific age groups. The development of normative data for specific age and disease groups will allow direct comparison of individual subjects with cortical thickness norms in health and disease. This process has the potential of aiding in the early diagnosis of dementia. Furthermore, unlike commonly used region of interest measures, cortical thickness analysis provides coverage of the complete cerebrum, and could thus be used for differential diagnosis of the various types of dementia as well. Finally, future studies will have to show the value of this new method in monitoring of the progression of dementia across the entire cortex.

Notes

ICBM grant PO1MHO52176-11, principal investigator Dr John Mazziotta; CIHR grant MOP-34996. Jason Lerch is funded by a K.M. Hunter/CIHR Doctoral Research Award.

Address correspondence to Alan C. Evans, McConnell Brain Imaging Centre, Montreal Neurological Institute, 3801 University Street, Montreal QC Canada H3A 2B4. Email: alan@bic.mni.mcgill.ca.

References

Ashburner J, Friston KJ (2000) Voxel-based morphometry — the methods. Neuroimage 11:805–821.

Baron JC, Chetelat G, Desgranges B, Perchey G, Landeau B, de la Sayette V, Eustache F (2001) *In vivo* mapping of gray matter loss with voxel-based morphometry in mild Alzheimer's disease. Neuroimage 14:298–309.

Braak H, Braak E (1991) Neuropathological stageing of Alzheimer-related changes. Acta Neuropathol (Berl) 82:239–259.

Braak H, Braak E (1996) Evolution of the neuropathology of Alzheimer's disease. Acta Neurol Scand Suppl 165:3–12.

Buckner RL, Snyder AZ, Sanders AL, Raichle ME, Morris JC (2000) Functional brain imaging of young, nondemented, and demented older adults. J Cogn Neurosci 12(Suppl 2):24–34.

Busatto GF, Garrido GE, Almeida OP, Castro CC, Camargo CH, Cid CG, Buchpiguel CA, Furuie S, Bottino CM (2003) A voxel-based morphometry study of temporal lobe gray matter reductions in Alzheimer's disease. Neurobiol Aging 24:221–231.

Callen DJ, Black SE, Gao F, Caldwell CB, Szalai JP (2001) Beyond the hippocampus: MRI volumetry confirms widespread limbic atrophy in AD. Neurology 57:1669–1674.

Chung M, Worsley K, Paus T, Robbins S, Evanc A, Taylor J, Giedd J, Rapoport J (2002) Tensor-based surface morphometry. Madison, WI: University of Wisconsin.

Collins DL, Neelin P, Peters TM, Evans AC (1994) Automatic 3-D intersubject registration of MR volumetric data in standardized Talairach space. J Comput Assist Tomogr 18:192–205.

Cronin-Golomb A, Corkin S, Rizzo JF, Cohen J, Growdon JH, Banks KS (1991) Visual dysfunction in Alzheimer's disease:relation to normal aging. Ann Neurol 29:41–52.

de Leon MJ, Convit A, DeSanti S, Bobinski M, George AE, Wisniewski HM, Rusinek H, Carroll R, Saint Louis LA (1997) Contribution of structural neuroimaging to the early diagnosis of Alzheimer's disease. Int Psychogeriatr 9(Suppl 1):183–90 [discussion 247–52].

De Toledo-Morrell L, Goncharova I, Dickerson B, Wilson RS, Bennett DA (2000) From healthy aging to early Alzheimer's disease: *in vivo* detection of entorhinal cortex atrophy. Ann N Y Acad Sci 911:240–253.

Fields SD, Fulop G, Sachs CJ, Strain J, Fillit H (1992) Usefulness of the Neurobehavioral Cognitive Status Examination in the hospitalized elderly. Int Psychogeriatr 4:93–102.

Fischl B, Dale AM (2000) Measuring the thickness of the human cerebral cortex from magnetic resonance images. Proc Natl Acad Sci USA 97:11050–11055.

Folstein MF, Folstein SE, McHugh PR (1975) 'Mini-mental state'. A practical method for grading the cognitive state of patients for the clinician. J Psychiatr Res 12:189–198.

Fox NC, Cousens S, Scahill R, Harvey RJ, Rossor MN (2000) Using serial registered brain magnetic resonance imaging to measure disease progression in Alzheimer disease: power calculations and estimates of sample size to detect treatment effects. Arch Neurol 57:339–344.

Genovese CR, Lazar NA, Nichols T (2002) Thresholding of statistical maps in functional neuroimaging using the false discovery rate. Neuroimage 15:870–878.

Gomez-Isla T, Hollister R, West H, Mui S, Growdon JH, Petersen RC, Parisi JE, Hyman BT (1997) Neuronal loss correlates with but exceeds neurofibrillary tangles in Alzheimer's disease. Ann Neurol 41:17–24.

Good CD, Scahill RI, Fox NC, Ashburner J, Friston KJ, Chan D, Crum WR, Rossor MN, Frackowiak RS (2002) Automatic differentiation of anatomical patterns in the human brain: validation with studies of degenerative dementias. Neuroimage 17:29–46.

Grignon Y, Duyckaerts C, Bennecib M, Hauw JJ (1998) Cytoarchitectonic alterations in the supramarginal gyrus of late onset Alzheimer's disease. Acta Neuropathol (Berl) 95:395–406.

Jones SE, Buchbinder BR, Aharon I (2000) Three-dimensional mapping of cortical thickness using Laplace's equation. Hum Brain Mapp 11:12–32.

Juottonen K, Laakso MP, Insausti R, Lehtovirta M, Pitkanen A, Partanen K, Soininen H (1998) Volumes of the entorhinal and perirhinal cortices in Alzheimer's disease. Neurobiol Aging 19:15–22.

Juottonen K, Laakso MP, Partanen K, Soininen H (1999) Comparative MR analysis of the entorhinal cortex and hippocampus in diagnosing Alzheimer disease. AJNR Am J Neuroradiol 20(1):139–44.

Kabani N, Le Goualher G, MacDonald D, Evans AC (2001) Measurement of cortical thickness using an automated 3-D algorithm: a validation study. Neuroimage 13:375–380.

Krasuski JS, Alexander GE, Horwitz B, Daly EM, Murphy DG, Rapoport SI, Schapiro MB (1998) Volumes of medial temporal lobe structures in patients with Alzheimer's disease and mild cognitive impairment (and in healthy controls). Biol Psychiatry 43:60–68.

Lerch JP, Evans AC (2004) Cortical thickness analysis examined through power analysis and a population simulation. Neuroimage (in press).

MacDonald D, Kabani N, Avis D, Evans AC (2000) Automated 3-D extraction of inner and outer surfaces of cerebral cortex from MRI. Neuroimage 12:340–356.

Matsuda H, Kitayama N, Ohnishi T, Asada T, Nakano S, Sakamoto S, Imabayashi E, Katoh A (2002) Longitudinal evaluation of both morphologic and functional changes in the same individuals with Alzheimer's disease. J Nucl Med 43:304–311.

McKhann G, Drachman D, Folstein M, Katzman R, Price D, Stadlan EM (1984) Clinical diagnosis of Alzheimer's disease:report of the NINCDS-ADRDA Work Group under the auspices of Department of Health and Human Services Task Force on Alzheimer's Disease. Neurology 34:939–944.

Miller MI, Massie AB, Ratnanather JT, Botteron KN, Csernansky JG (2000) Bayesian construction of geometrically based cortical thickness metrics. Neuroimage 12:676–687.

Mori E, Yoneda Y, Yamashita H, Hirono N, Ikeda M, Yamadori A (1997) Medial temporal structures relate to memory impairment in Alzheimer's disease:an MRI volumetric study. J Neurol Neurosurg Psychiatry 63:214–221.

Mungas D, Reed BR, Jagust WJ, DeCarli C, Mack WJ, Kramer JH, Weiner MW, Schuff N, Chui HC (2002) Volumetric MRI predicts rate of cognitive decline related to AD and cerebrovascular disease. Neurology 59:867–873.

Nagy Z, Hindley NJ, Braak H, Braak E, Yilmazer-Hanke DM, Schultz C, Barnetson L, Jobst KA, Smith AD (1999) Relationship between clinical and radiological diagnostic criteria for Alzheimer's disease and the extent of neuropathology as reflected by 'stages': a prospective study. Dement Geriatr Cogn Disord 10:109–114.

Pinheiro JC, Bates DM (2000) Mixed-effects models in S and S-PLUS. New York: Springer.

Pruessner JC, Collins DL, Pruessner M, Evans AC (2001) Age and gender predict volume decline in the anterior and posterior hippocampus in early adulthood. J Neurosci 21:194–200.

Pruessner JC, Kohler S, Crane J, Pruessner M, Lord C, Byrne A, Kabani N, Collins DL, Evans AC (2002) Volumetry of temporopolar, perirhinal, entorhinal and parahippocampal cortex from high-resolution MR images: considering the variability of the collateral sulcus. Cereb Cortex 12:1342–1353.

Prvulovic D, Hubl D, Sack AT, Melillo L, Maurer K, Frolich L, Lanfermann H, Zanella FE, Goebel R, Linden DE, Dierks T (2002) Functional imaging of visuospatial processing in Alzheimer's disease. Neuroimage 17:1403–1414.

Rizzo M, Anderson SW, Dawson J, Nawrot M (2000) Vision and cognition in Alzheimer's disease. Neuropsychologia 38:1157–1169.

Rosas HD, Liu AK, Hersch S, Glessner M, Ferrante RJ, Salat DH, van der Kouwe A, Jenkins BG, Dale AM, Fischl B (2002) Regional and progressive thinning of the cortical ribbon in Huntington's disease. Neurology 58:695–701.

Scahill RI, Schott JM, Stevens JM, Rossor MN, Fox NC (2002) Mapping the evolution of regional atrophy in Alzheimer's disease:unbiased analysis of fluid-registered serial MRI. Proc Natl Acad Sci USA 99:4703–4707.

Scahill RI, Frost C, Jenkins R, Whitwell JL, Rossor MN, Fox NC (2003) A longitudinal study of brain volume changes in normal aging using serial registered magnetic resonance imaging. Arch Neurol 60:989–994.

Sled JG, Zijdenbos AP, Evans AC (1998) A nonparametric method for automatic correction of intensity nonuniformity in MRI data. IEEE Trans Med Imaging 17:87–97.

Small GW, Agdeppa ED, Kepe V, Satyamurthy N, Huang SC, Barrio JR (2002) *In vivo* brain imaging of tangle burden in humans. J Mol Neurosci 19:323–327.

Thompson KM (1989) Effects of early alcohol use on adolescents' relations with peers and self-esteem: patterns over time. Adolescence 24:837–849.

Thompson PM, Mega MS, Woods RP, Zoumalan CI, Lindshield CJ, Blanton RE, Moussai J, Holmes CJ, Cummings JL, Toga AW (2001) Cortical change in Alzheimer's disease detected with a disease-specific population-based brain atlas. Cereb Cortex 11:1–16.

Thulborn KR, Martin C, Voyvodic JT (2000) Functional MR imaging using a visually guided saccade paradigm for comparing activation patterns in patients with probable Alzheimer's disease and in cognitively able elderly volunteers. AJNR Am J Neuroradiol 21: 524–531.

Valla J, Berndt JD, Gonzalez-Lima F (2001) Energy hypometabolism in posterior cingulate cortex of Alzheimer's patients:superficial laminar cytochrome oxidase associated with disease duration. J Neurosci 21:4923–4930.

Van Hoesen GW (1995) Anatomy of the medial temporal lobe. Magn Reson Imag 13:1047–1055.

Van Hoesen GW, Parvizi J, Chu CC (2000) Orbitofrontal cortex pathology in Alzheimer's disease. Cereb Cortex 10:243–251.

Xu Y, Jack CR Jr, O'Brien PC, Kokmen E, Smith GE, Ivnik RJ, Boeve BF, Tangalos RG, Petersen RC (2000) Usefulness of MRI measures of entorhinal cortex versus hippocampus in AD. Neurology 54: 1760–1767.

Yezzi AJ Jr, Prince JL (2003) An Eulerian PDE approach for computing tissue thickness. IEEE Trans Med Imaging 22:1332–1339.

Zeng X, Staib LH, Schultz RT, Duncan JS (1999) Segmentation and measurement of the cortex from 3-D MR images using coupled-surfaces propagation. IEEE Trans Med Imag 18:927–937.

Zijdenbos AP, Forghani R, Evans AC (2002) Automatic 'pipeline' analysis of 3-D MRI data for clinical trials: application to multiple sclerosis. IEEE Trans Med Imag 21:1280–1291.